Structure Change from Bet -Strand and Turn to alpha-Helix in Histone H2A-H2B Induced by DNA Damage Response

Y Izumi, F Fujii, F Wien, C Houée-Lévin, S Lacombe, D Salado-Leza, E Porcel, R Masoud, S Yamamoto, Matthieu M. Refregiers, et al.

Structure change from β-strand and turn to α-helix in histone H2A-H2B induced by DNA damage response

Y. Izumi,* K. Fujii, F. Wien, C. Houée-Lévin, S. Lacombe, D. Salado-Leza, E. Porcel, R. Masoud, S. Yamamoto, M. Réfrégiers, M. –A. Hervé du Penhoat, and A. Yokoya

*Corresponding author

Abstract

Using synchrotron radiation based circular dichroism spectroscopy, we found that the DNA damage response (DDR) induces an increase of α-helix structure and a decrease of β-strand and turn structures in histone H2A-H2B extracted from X-irradiated human HeLa cells. The structural alterations correspond to an assumption that an average of eight amino acid residues form new α-helix structures at 310 K. We propose the structural transition from β-strand and turn structures to an α-helix structure in H2A-H2B as a novel process involved in DDRs.

Keywords

Synchrotron radiation, circular dichroism, chromatin remodeling, post-translational modification, DNA repair, histone dynamics

Introduction

DNA wraps around core histones composed of H2A, H2B, H3, and H4 subunits in eukaryotic nuclei. In recent years, histones have been shown to play a substantial role in gene regulation and epigenetic silencing. Posttranslational modifications of histones are involved not only in regulating DNA replication and transcription but also in repairing harmful DNA damage caused by various stress factors, such as endogenously arising reactive oxygen species (1) and ultraviolet (UV) (2) and ionizing radiation (3). These factors lead to various types of DNA damage, such as the modification of bases, formation of DNA adducts, cross-linking of the DNA strands, and production of single- and double-strand breaks (DSBs) (4). DSBs are particularly harmful types of DNA damage. When DSBs are induced in the genome, they may lead to discontinuous DNA and a loss of genetic information, resulting in mutations or ultimately to carcinogenesis if they are not properly removed from the genome by certain enzymatic systems. To avoid this, cells have evolved DNA damage response (DDR) mechanisms, including DNA repair and cell-cycle regulation.

DNA repair processes have been studied and reviewed well elsewhere (4–11). It has been shown that sequential recruitment of DSB-repair proteins and posttranslational modification of histones are preferentially induced at the early stage of DSB repair processes. The MRN complex, consisting of Mre11, Rad50, and Nbs1 proteins, binds to the DSB site and recruits ATM protein kinase (12). The ATM phosphorylates the serine 139 residue of histone H2AX, which is a variant of H2A, in the vicinity of the DSB site (13). The phosphorylated H2AX, which is well known as γ-H2AX, binds to MDC1 protein to create a docking site for an additional MRN-ATM complex (14). The additional ATM further phosphorylates proximal H2AX around the DSB site (15). This cycle leads to the formation of a megabase-sized γ-H2AX domain surrounding the DSB site, which is microscopically observed as γ-H2AX foci (16). TIP60 is also recruited and acetylates γ-H2AX. It associates with the E2 ubiquitin-conjugating enzyme UBC13 to regulate polyubiquitination of acetylated γ-H2AX (17). Polyubiquitinated and acetylated γ-H2AX is removed from chromatin. The MDC1 protein is also phosphorylated by ATM (18–20) and recruits the RNF8-UBC13 complex to ubiquitinate H2A(X) (20–22). The E3 ubiquitin ligase RNF168 binds to these ubiquitinated H2A(X) and promotes the formation of ubiquitin conjugates (23). BRCA1, which is one of the most important tumor-suppressing factors involved in DNA repair, binds to the polyubiquitinated histone through RAP80 and locates near the DSB site (24–26). These events facilitate DSB repair and/or the cell-cycle checkpoint. After accumulation of the repair proteins, DSB repair proceeds through two distinct mechanisms, the nonhomologous end joining (NHEJ) and homologous recombination (HR) pathways (9–11). NHEJ involves minimal processing of the damaged by nucleases, followed by direct

religation of the damaged DNA ends. It can be used in all cell-cycle phases, but it is an error-prone repair pathway. In contrast, although HR is error free, it requires adjacent sister chromatids, which are only present during the S and G2phases, for homology searching, and therefore it is restricted during those phases.

The access/prime-repair-restore model (27,28) is a well-known view of the chromatin remodeling induced by DDRs, including DNA damage repair processes. It predicts that core histone proteins are displaced from chromatin around DNA damage sites to give the DNA repair proteins access to the damage site before the repair process, and are repositioned after the repair is completed. Some experimental results seem to be consistent with the model, as reviewed by Polo (29). For example, the eviction of H2A-H2B dimer from chromatin occurs within 30 min after induction of DSB, but the histone level around DSB sites returns to normal within 2 h after DSB induction (30). However, the chromatin remodeling processes have not yet been explained completely, and the dynamics of histone during DDRs is still an open question.

Recently, by measuring UV circular dichroism (CD) spectra, we found that secondary-structure alterations of H2A and H2B (H2A-H2B) are induced in x-ray-irradiated human cultured cells (31). This alteration is thought to be strongly involved in DDR processes, but its role has not yet been identified. To clarify this role, it is important to investigate the alterations of H2A-H2B more precisely and examine the dynamics of the structural change in terms of the thermodynamic properties of the proteins.

In this work, we extended the CD measurement range to the vacuum UV (VUV) region (wavelength < ~200 nm) using a synchrotron radiation-based CD spectroscopy system. The structural information obtained with this setup is more precise because additional CD peaks of proteins can be observed in the VUV region. Based on the experimental results, we propose the transition from β-strand and turn structures to an α-helix structure in H2A-H2B as a novel, to our knowledge, process involved in DDRs. In addition, we determined thermodynamic parameters that relate to the dynamics of H2A-H2B (namely, enthalpy, entropy, and Gibbs energy changes) by analyzing the CD spectra as a function of temperature.

Materials and methods

Sample preparation

The sample preparation procedures are described in our previous paper (31). Briefly, human cancer cells (HeLa.S-FUCCI cells, provided by the RIKEN cell bank), were cultured in 100-mm cell culture dishes (Corning , Corning, NY). The density of the cultured cells was

~1 × 10^7cells/dish. Dulbecco's modified Eagle's medium (Wako Pure Chemical Industries, Osaka, Japan) supplemented with 10% fetal bovine serum (Biological Industries, Beit Haemek, Israel) and 1% antibiotic-antimycotic solution (Life Technologies, Grand Island, NY) was used for cell culture. Incubation was carried out at 310 K in a humidified atmosphere of 5% CO_2 and 95% air.

Cells were irradiated in the culture dishes with X-rays for 20 minutes using an X-ray generator equipped with a tungsten anode (M-150WE: SOFTEX, Kanagawa, Japan). The tube voltage and current were set at 150 kV and 6 mA, respectively. The energies of the characteristic x-rays emitted from the tungsten anode were 59.318 ($K_{\alpha 1}$ line), 57.982 ($K_{\alpha 2}$ line), 67.244 ($K_{\beta 1}$ line), and 69.067 ($K_{\beta 2}$ line) keV (32). An aluminum filter (0.2 mm thick) was used to reduce the low-energy component to <10 keV. The dose rate was estimated to be ~2 Gy/min using a Fricke dosimeter. The chemical yield of the dosimeter G(Fe^{3+}) at ~60 keV, with a value of 14.5 (33), was used to calculate the dose rate because the $K_{\alpha 1}$ line is the most intense emission (32). An x-ray dose of 40 Gy is thought to produce ~1600 DSBs per cell nucleus (3). Assuming that the DSBs are randomly spaced in DNA, the average DNA fragment length is ~2 Mbp because the human genome is ~3000 Mbp. Since phosphorylation of H2AX, which is a variant of H2A and is known as γ-H2AX, occurs in the early stage of DNA repair processes and spreads along ~2 Mbp (34), it is expected that most histones in x-irradiated cells are involved in DDRs. After irradiation, the cells were incubated for 30 min in the above-mentioned condition to allow for DNA repair processes.

A pellet containing H2A-H2B was obtained from x-irradiated or unirradiated cells using a Histone Purification Kit (Active Motif, Carlsbad, CA) and dissolved with sterile water. The kit is designed to extract H2A-H2B from core histones in chromatins while maintaining the posttranslational modification of H2A-H2B induced by cellular functions such as DNA repair processes. Centrifugal filtration of the aqueous solution was carried out to remove the remaining nucleic acids using a Nanosep centrifugal device (OD010C34; Pall, Port Washington, NY) with a molecular mass cutoff of 10 kDa. The remaining aqueous solution on the filter after centrifugation was collected. We confirmed that the amount of DNA with a molecular mass of >10 kDa that remained in the collected solution was negligible (~0.5% of histones) by using a Qubit dsDNA BR Assay Kit, a Qubit ssDNA Assay Kit, and a Qubit Protein Assay Kit (ThermoFisher Scientific, Boston, MA).

Tris-HCl buffer and sodium fluoride (NaF) were added to each sample to induce the formation of higher-order structures. The final concentrations of H2A-H2B, Tris-HCl, and NaF were 3.6×10^{-4} M, 10 mM, and 250 mM, respectively. The molar concentration C of the

H2A-H2B samples was determined by using Beer-Lambert's law: $C = A/(\varepsilon L)$, where A is the absorbance at 280 nm, ε is the molar absorption coefficient of H2A-H2B extracted from unirradiated cells at 280 nm (10700 M^{-1} cm^{-1}, determined prior to this work (31)), and L is the path length in centimeters. Although H2A-H2B extracted from x-irradiated cells contained modified histones produced during the DNA repair processes, we ignored the effect of these modifications on the absorbance because we did not observe significant differences between the absorption spectra of irradiated and unirradiated samples in the UV region. A microvolume spectrophotometer (NanoDrop 2000 UV-Vis spectrophotometer; ThermoFisher Scientific) was used for absorption spectroscopy. The molar concentration C of the H2A-H2B samples was double-checked using the Qubit Protein Assay Kit. No aggregation of proteins was observed in dynamic light scattering (DLS) measurements. A light-scattering detector (Zetasizer μV; Malvern Instruments, Worcestershire, UK) was used for DLS measurements.

Electrophoresis and Western blotting

Histone protein samples were analyzed by sodium dodecyl sulfate-polyacrylamide gel electrophoresis (SDS-PAGE) analysis to confirm their purity, and component changes of H2A-H2B induced by x-irradiation of the cells using NuPAGE 12% Bis-Tris gels in MES running buffer (Life Technologies). Protein bands were stained using an Oriole fluorescent gel stain (Bio-Rad Laboratories, Hercules, CA). Images were taken using an Ettan DIGE Imager (GE Healthcare, Buckinghamshire, UK).

To confirm replacement of H2A with its variant H2AZ, which is known to occur during DNA repair processes (4), we also performed Western blot analyses using chemiluminescence according to a protocol provided by Cell Signaling Technology. A primary antibody, histone H2A.Z antibody (Cell Signaling Technology, Danvers, MA), was used at 1:1000 dilution. A secondary antibody, anti-rabbit IgG HRP-linked antibody (Cell Signaling Technology), was used at 1:2000 dilution. Images were taken using a LumiCube chemiluminescence analyzer (Liponics, Tokyo, Japan).

CD spectroscopy and analyses

CD spectroscopy was carried out at the DISCO beamline of Synchrotron SOLEIL (Gif-sur-Yvette, France) (35). Two microliters of sample was encapsulated in a calcium fluoride (CaF_2) sample cell. The path length of the CaF_2 cell was 12 μm. The CD intensity was calibrated using (+)-10-camphorsulfonic acid (Sigma-Aldrich, St. Louis, MO). CD spectra were measured between 175 and 260 nm. The sample temperature was controlled between 288 and 338 K. The pH of the sample solvent (Tris-HCl and NaF) changed from 8.6 to 7.3 during the temperature increase. However, it was previously shown that the CD spectra

of unirradiated H2A-H2B do not depend on pH in the 5.5–10.5 pH range (36). To ensure reproducibility, we measured the CD spectra three times using samples extracted from HeLa cells of different passages. The spectral shapes were similar in each experimental condition. We also measured the CD spectrum of the sample solvent (baseline spectrum) to evaluate pseudo CD signals that might originate from, e.g., the optical systems and CaF_2 cells used. After subtracting the baseline spectrum from the CD spectra of H2A-H2B, we carried out the analyses described below.

The CD spectra with subtracted baselines were then converted to molar CD $\Delta\varepsilon$ (M^{-1} cm^{-1}) to analyze the contents of the secondary structures. Molar CD $\Delta\varepsilon$ is defined as

$$\Delta\varepsilon = \theta / (32980\, C\, N\, l), \quad \text{(Eq. 1)}$$

where θ, C, N, and l are the CD intensity described as ellipticity in millidegrees, the molar concentration of H2A-H2B (as defined above), the number of amino acid residues, and the path length of the CaF_2sample cell in centimeters, respectively. In this study, N is assumed to be equal to the average number of H2A and H2B residues (N = 127). The contents in secondary structures of the samples were analyzed using the BeStSel program (37), applied at a wavelength range between 180 and 250 nm.

To examine the structural alterations of H2A-H2B thermodynamically, we calculated ΔG from the temperature dependence of the CD intensity (20). The Gibbs energy change is defined as

$$\Delta G(T) = -RT \ln K = -RT \ln \frac{\mathrm{CD}(T) - \mathrm{CD}_{initial}}{\mathrm{CD}_{final} - \mathrm{CD}(T)}, \quad \text{(Eq. 2)}$$

where R, CD(T), $CD_{initial}$, and CD_{final} correspond to the gas constant and the CD intensities at the sample temperature T, of the intiial form and of the final form, respectively. In this work, we monitored the temperature dependence of the CD intensity at 222 nm because the highest content of secondary structure in the sample was α-helix at 288 K (see details in the "Secondary-structure change" section below) (38). The midpoint transition T_m (i.e., the temperature at which $\Delta G = 0$) was determined by using the method of weighted least squares. Since $\Delta G$is defined to be $\Delta G = \Delta H - T\Delta S$, we can convert Eq. 2 to

$$R \ln K = -\Delta H\left(\frac{1}{T}\right) + \Delta S . \quad \text{(Eq. 3)}$$

Using the weighted least squares method, we also determined the enthalpy ΔH and entropy ΔS changes.

Results and Discussion

SDS-PAGE and Western blotting

Fig. 1*a* shows a representative SDS-PAGE result, comparing samples from 40 Gy irradiated cells and unirradiated cells. Two bands were observed at ~15 kDa in both the unirradiated and irradiated samples (lanes U and I, respectively). The lower bands were assigned to be H2A based on the results from SDS-PAGE for recombinant H2A (New England BioLabs, Ipswich, MA) carried out prior to this work (Fig. S1 in the Supporting Material). Western blot analysis using the H2AZ antibody showed that both samples contained H2AZ (Fig. 1*b*). Presumably, these samples would also contain other variants of H2A, such as H2AX, and posttranslationally modified forms of H2A and its variants, such as phosphorylated, acetylated, and methylated forms. Since the other bands observed at ~15 kDa were assigned to be H2B based on the SDS-PAGE result for recombinant H2B (New England BioLabs) (Fig. S1), the samples presumably would also contain the variants and modified forms of H2B. Bands at ~20 kDa were observed in both SDS-PAGE and Western blot analyses (Fig. 1, *a* and *b*). Since a band at ~20 kDa was also observed in a Western blot analysis using ubiquitin antibody carried out prior to this work (Fig. S2), these bands were assigned to be monoubiquitinated H2AZ (uH2AZ). Since ~5–10% of H2A is monoubiquitinated in mammalian cells even under normal conditions (39), it is natural to think that the samples contained not only uH2AZ but also monoubiquitinated H2A (uH2A). Indeed, similar results were observed in the Western blot analyses using H2A and ubiquitin antibodies (40).

When we compared the fluorescence intensities obtained by densitometric analysis of the gel images of H2A(Z), uH2A(Z), and H2B bands in the irradiated sample with those in the unirradiated sample, we observed no apparent difference. In addition, we observed no band below that of H2A in the irradiated sample (Fig. 1*a*). These results suggest that 1) decomposition of histone proteins in x-irradiated cells was hardly induced, and 2) ubiquitination of histones scarcely occurred during or after x-irradiation of the cells in our samples. Furthermore, we observed no apparent difference in the fluorescence intensity of H2AZ between the two samples (Fig. 1*b*), which suggests that replacement of H2A with H2AZ also scarcely occurred in our samples.

The band of H4 would appear approximately halfway between 10 and 15 kDa (Fig. S3) in our experimental conditions. However, no band was observed below that of H2A in the gel of the

two samples, as mentioned above (Fig. 1*a*), and therefore our CD samples did not contain H4. Similarly, the band of H3 would appear slightly below the band of H2B (Fig. S3) in our experimental conditions. If our samples contained H3, the band of H2B assigned as described above would be broader than that of H2A. However, the bandwidths of H2A and H2B were almost the same in each sample. Thus, the contamination of H3 was also negligible in our samples. Slight bands were observed between 25 and 50 kDa, as shown in Fig. 1*a*. Bands between 25 and 40 kDa were also observed even in the case of recombinant H2A (Fig. S1). Therefore, these bands would originate from some kind of complex of H2A and its variants that formed during the SDS-PAGE analyses, because no aggregation was observed in the DLS measurements as mentioned above. We could not find any candidates for the other bands observed between 40 and 50 kDa. The fluorescence intensities of these slight bands between 25 and 50 kDa of the unirradiated sample differed from those of the irradiated sample. Nevertheless, since the sum of the fluorescence intensities of the bands of H2A(Z), uH2A(Z), and H2B was ~10 times larger than that of the bands between 25 and 50 kDa, the effects of unidentified molecules observed as bands between 25 and 50 kDa are negligible in the CD spectra measurements.

CD-spectra change

Fig. 2 shows the CD spectra of H2A-H2B extracted from unirradiated and irradiated cells measured at 294, 310 (body temperature), and 330 K. A CD spectrum of H2A-H2B irradiated with 40 Gy x-rays after extraction from unirradiated cells (31) is also shown (described as x-irradiated H2A-H2B). This spectrum was measured at 294 K using a commercial CD spectrometer (J-725; JASCO, Tokyo, Japan), limiting the measurements to the UV region (wavelength > ~195 nm). The conformation of most of the H2A-H2B molecules was estimated to be folded at 294 K and unfolded at 330 K based on the temperature dependence of the intensity of the CD spectra (see further details in the "Thermodynamic parameters of H2A-H2B" section below). At 294 K (Fig. 2*a*), the CD spectra of H2A-H2B extracted from unirradiated and irradiated cells showed a positive peak at ~190 nm and two negative ones at ~208 and 222 nm. These peaks are characteristic of the CD peaks of α-helix structures (41). The absolute values of the CD peak intensities of H2A-H2B were higher for irradiated cells than for unirradiated ones, which is consistent with our previous work carried out at 294 K in only the UV region (wavelength > ~195 nm) (13). In contrast, the absolute values of the CD intensities were lower for x-irradiated H2A-H2B than for the unirradiated sample (*blue line* in Fig. 2*a*). This alteration could be caused by x-ray-induced peptide damage (or cleavage) (42). Thus, these results suggest that the secondary-structure alterations observed in H2A-H2B extracted from irradiated cells could be ascribed not to x-ray damage to H2A-H2B itself but to some cellular responses to irradiation stress, such as chemical modification induced by enzymatic reactions before or during DNA damage repair processes. Similar spectral changes were observed at 310 and 330 K

(Fig. 2, *b* and *c*). These CD-spectra changes show that secondary-structure alterations of H2A-H2B were also induced in the x-irradiated cells. As shown in Fig. 2, thermal elevation reduced the CD peak intensities for both irradiated and unirradiated samples. A wavelength blue shift for all peaks was also observed. These spectral changes reflect the transition to other structural states at higher temperatures.

Secondary-structure change

Fig. 3 shows the temperature dependence of each secondary-structure content, which we determined by analyzing the variation of the molar CD, $\Delta\varepsilon$, with wavelength, using the BeStSel program (37) for H2A-H2B extracted from unirradiated and x-irradiated cells. The secondary-structure contents of x-irradiated H2A-H2B at 294 K are also shown. It should be noted that some contents originated from ubiquitin in ubiquitinated H2A, which is produced during the DNA damage repair process (22) and is contained in mammalian cells even under normal conditions (21). In our previous study, we concluded that this contribution is minor (31).

The α-helix content of the unirradiated sample is consistent with previous data that we reanalyzed (31,43) using the BeStSel program (19) (Fig. 3*a*). On the other hand, the α-helix content of the native form at 288 K (Fig. 3*a*) was less than the sum of the α-helix contents of H2A and H2B in the nucleosome determined by Davey et al. (44) using x-ray crystallography (~50%). The agreement is fairly reasonable (43) even though our study and that of Davey et al. (44) differ in terms of the experimental conditions used and the origin of the histones; for example, Davey et al. analyzed *Xenopus laevis* core histones together with a 146 bp palindromic DNA fragment in the crystal structure.

The α-helix and β-strand contents depended on temperature (Fig. 3, *a* and *b*). The α-helix content decreased and β-strand content increased with temperature elevation. A comparison of unirradiated and irradiated samples clearly demonstrates that x-ray irradiation of cells caused an increment of α-helix and a decrement of β-strand contents in the temperature range investigated (Fig. 3, *a* and *b*). As for the turn structure (Fig. 3*c*), no apparent temperature dependence was observed in either sample, although a decrement of turn content was induced by x-ray irradiation of cells. Other structures, including the 3_{10}-helix, π-helix, β-bridge, bend, loop/irregular, and invisible regions of the structures (Fig. 3*d*) (37), showed a similar temperature dependence for both irradiated and unirradiated H2A-H2B, and no apparent change was induced by x-ray irradiation of cells (Fig. 3d). In contrast, in the case of x-irradiated H2A-H2B measured at 294 K, a decrement of α-helix and an increment of β-strand and turn contents were observed compared with the unirradiated sample. This result is the opposite of what was observed in the case of x-irradiation of cells. Since, as

mentioned above, structural alterations of x-irradiated H2A-H2B would be induced by x-ray damage to H2A-H2B itself, the structural alterations observed in H2A-H2B extracted from irradiated cells (i.e., the increment of α-helix and the decrement of β-strand and turn structures) were due to some cellular responses to irradiation stress. Altogether, these results suggest that the β-strand and turn structures transitioned to α-helix structures in H2A-H2B during DDRs (see details below).

Possible mechanisms of the α-helix increment

At body temperature (310 K), the α-helix content increased from 18.7% to 25.0% (a 6.3% increment) during DDRs (Fig. 3a). In this section, we discuss several structure-alteration mechanisms that might explain our results, focusing on changes in the total number of amino acid residues that formed α-helix structures.

Replacement of H2A with H2AZ

It is known that H2A is replaced by H2AZ during DNA repair processes (4), as mentioned above. this could be one of the possible mechanisms of the secondary-structure change, since the contents of the primary and secondary structures differ between H2A and H2AZ (44,45). To test this hypothesis, we calculated the number of amino acid residues forming α-helix structures in H2AZ required to explain the increment of α-helix content observed in this work, even though we did not observe an apparent replacement of H2A by H2AZ in this work.

The numbers of molecules of H2A, H2B, and H2AZ in the sample were defined as n_a, n_b, and n_z, respectively. The total numbers of amino acid residues that formed the α-helix structures per molecule were defined as h_a for H2A, h_b for H2B, and h_z for H2AZ. For the sake of simplicity, we assume that the unirradiated sample contained only H2A and H2B molecules. The α-helix content of the unirradiated sample H_{unirrad}, i.e., the α-helix content before replacement, is described as

$$H_{unirrad} = \frac{h_a n_a + h_b n_b}{129 n_a + 125 n_b} = 0.187 , \quad \text{(Eq. 4)}$$

where digits 129 and 125 in the denominator are the numbers of amino acid residues in an H2A and an H2B molecule, respectively (47). It should be noted that the initiator methionine was excluded from the estimation because it is removed after translation in cells (48). Even if it is included, the conclusion is not affected significantly. Assuming that some H2A molecules are replaced by H2AZ molecules during DDRs, we can describe the α-helix

content of the irradiated sample, H_{irrad}, as

$$H_{irrad} = \frac{h_a(n_a - n_z) + h_b n_b + h_z n_z}{129(n_a - n_z) + 125 n_b + 127 n_z} = 0.250\,, \qquad \text{(Eq. 5)}$$

where digit 127 in the denominator is the number of amino acid residues in an H2AZ molecule (4). Using equations Eqs 4 and 5, we obtain

$$n_z = \frac{16.002}{h_z - h_a + 0.5} n_a\,, \qquad \text{(Eq. 6)}$$

where we assume that $n_a = n_b$, because H2A and H2B molecules exist as dimers in the core histone. Since we assume that H2A is replaced by H2AZ, n_z must be lower than or equal to n_a ($n_a \geq n_z$). Finally, we find that

$$h_z \geq h_a + 15.502\,. \quad \text{(Eq. 7)}$$

X-ray crystallographic data show that h_z (= 56) is similar to h_a (= 57) (45, 46). Although there are no data for h_z and h_a in solution at 310 K, it seems very unlikely that h_z would be ≥16 amino acid residues larger than h_a at this temperature. At other temperatures (288-338 K) and considering experimental errors, similar results are obtained.

Thus, the replacement of H2A with H2AZ does not explain the increment of α-helix structures.

Ubiquitination

H2A and H2B molecules are known to be ubiquitinated during DNA repair processes (49). Ubiquitin is a small protein (76 residues) and has α-helix and other structures (50). When H2A molecules are ubiquitinated, the contents of secondary structures should change. Although an apparent increment of ubiquitinated H2A is not observed in Fig. 1a, we evaluated the possibility that ubiquitination contributed to the experimental results.

Using the same formalism, we defined the number of amino acid residues that formed α-helix structures in a ubiquitin molecule as h_u and the number of ubiquitin molecules as n_u. If we assume that the increment of α-helix content originates only from ubiquitination of H2A, we may describe the α-helix content of irradiated sample as follows:

$$H_{irrad} = \frac{h_a n_a + h_b n_b + h_u n_u}{129 n_a + 125 n_b + 76 n_u} = 0.250\,, \qquad \text{(Eq. 8)}$$

where 76 in the denominator is the number of amino acid residues of ubiquitin. It should be noted that equation (Eq. 8) is also true if H2B or both histones are ubiquitinated. Using equations Eq. 4 and 8, we can obtain

$$n_u = \frac{16.002}{h_u - 19} n_a , \quad \text{(Eq. 9)}$$

where we assume that $n_a = n_b$. To satisfy n_a and $n_u \geq 0$, h_u must be larger than 19. Both X-ray crystallographic experiment (50) and CD spectroscopy (51) carried out in solution at 277 K have shown that h_u is smaller than 19 (h_u = 12 in both cases). Although the value of h_u in solution at 310 K is unknown, it would not exceed 19. At other temperatures (288-338 K) and considering experimental errors, similar results were obtained.

Thus, the ubiquitination of H2A induced by DNA damage repair processes cannot explain the increment of α-helix content.

Structure transition from β-strand and turn structures to α-helix

In this work, we observed an increment of *α*-helix structures and a decrement of *β*-strand and turn structures (Fig. 3). We hypothesize that the *β*-strand and turn structures changed to *α*-helix structures during DDRs. In this section, we analyze our results based on this hypothesis.

If we assume that *α*-helical transitions occur in all H2A and H2B molecules equally, we may describe the *α*-helix content of irradiated sample H_{irrad} as

$$H_{irrad} = \frac{h_a n_a + h_b n_b + x(n_a + n_b)}{129 n_a + 125 n_b} = 0.250 , \quad \text{(Eq. 10)}$$

where x is the total number of amino acid residues composing α-helix newly formed in an H2A and an H2B molecule by DDRs. Using equations Eq. 4 and 10 and assuming that $n_a = n_b$, we obtain

$$x = 8.001 . \quad \text{(Eq. 11)}$$

This analysis fits with the experimental results if an average of only eigth residues of β-strand or turn structures in unirradiated H2A-H2B transform into α-helix. At other temperatures, the values of x are approximately 4-12. Although the normal histone structures and altered parts for each temperature have not yet been identified, transition of an average of 4-12 residues can be realized by counting the number of residues that consist of β-strand and turn structures, as determined by X-ray crystallographic studies (45) and calculating them using our experimental data for each temperature.

Thus, based on the assumptions described in this section and on our experimental results, we propose the structural transition from β-strand and turn structures to α-helix of H2A-H2B as a novel, to our knowledge, process involved in DDRs.

Thermodynamic parameters of H2A-H2B

Figures 4(a) and its inset show the temperature dependence of the CD intensity at 222 nm for both samples and a magnification between 320 and 334 K for the unirradiated sample, respectively. In the case of the unirradiated sample, we observed two thermal transitions; one between ~292 and ~318 K (denoted as the lower transition) and one between ~322 and ~330 K (denoted as the higher transition). Focusing on the higher transition (see the inset of Fig. 3(a)),we found that the temperature at the midpoint of the transition was approximately 326 K. A similar value was reported by Karantza *et al*. (36). This transition could originate from thermal denaturation of H2A-H2B. This higher transition was not apparent in the irradiated sample (Fig. 4(a)), since the experimental data obtained from irradiated samples had greater variability than those obtained from unirradiated ones. This variability could originate not only from cell-to-cell variations in DNA damages but also from variability in the histone isomer composition of the nucleosome. In contrast, the lower transition was observed in both samples (Fig. 4(a)). Since the lower transition seems to differ from higher one, it may originate from other processes, such as partial extension and/or dissociation of H2A-H2B due to an increment in thermal energy.

Figure 4(b) shows Gibbs energy change (ΔG) of the lower transition calculated by using equation (Eq. 2). The corresponding curves of the best fit (see Materials and methods) are also shown. In this work, we defined $CD_{initial}$ and CD_{final} as the average of the CD intensities at 288 and 290 K and at 320 and 322 K, respectively. we did not observe an apparent difference between the ΔG values of the unirradiated and irradiated samples. The T_m values of the unirradiated and the irradiated samples were found to be 304.3±0.3 and 305.2±0.7 K, respectively, which are not significantly different. The thermodynamic parameters determined by the best fit using equation (Eq. 3) are listed in Table 1. The values determined for enthalpy and entropy changes in the irradiated sample were found to be lower than those obtained in the unirradiated sample. This suggests that the increase of α-helix content due to DDRs is related to a reduction of both enthalpy and entropy. A similar result was obtained in the case of a helix transition from a random coil of glutamic acid or lysine peptides (52). The decrease of entropy could be caused by helix formation, because it would reduce the disorder of H2A-H2B molecules. The enthalpy may decrease to compensate for the energetic stability of altered H2A-H2B.

A hypothesis regarding the structure-alteration mechanism

The details of how β-strand and turn structures change to a α-helix structure, and how this structural alteration contributes to the DNA repair process remain to be determined. We assume that an alteration mechanism would function via posttranslational modifications such as acetylation, methylation, and phosphorylation, which occur during DNA repair processes (45). These modifications would alter the steric barrier and/or electrostatic interaction

between modified residues and other residues, and possibly change the stable structure as a result. Indeed, acetylation of H4 has been shown to increase α-helix content (52).

Conclusion

We measured CD spectra of H2A-H2B extracted from x-irradiated and unirradiated human cancer cells in the UV-to-VUV region. An increment of α-helix structure and a decrement of β-strand and turn structures of H2A-H2B were induced by x-ray irradiation of cells. The structural alteration observed in this work corresponds to the assumption that, on average, 4–12 amino acid residues that form β-strand or turn structures in native H2A-H2B transform into α-helix structures. Thus, we propose the structural transition from β-strand and turn structures to α-helix of H2A-H2B as a novel, to our knowledge, process involved in DDRs.

It is known that mammals have two distinct DSB repair mechanisms, namely, the NHEJ and HR pathways, as mentioned in the Introduction. The NHEJ and HR pathways predominate in the G_1 phase and the S and G_2 phases of the cell cycle, respectively (9–11). The structural alterations induced by DDRs may depend on the cell cycle. The HeLa.S-FUCCI cells used in this work allow one to distinguish the cell cycle in real time because they can express genetically encoded fluorescent probes that effectively label individual G_1 phase nuclei red and S, G_2, and M phase nuclei green (53). Thus, we plan to compare the structural alterations that occur in each phase in a future study. When the causes of these alterations are identified, the dynamics of the H2A-H2B alteration will be revealed more precisely. In view of study for DDR, this is a very interesting and important topic for future work.

Author contributions

Y. I. prepared the samples, carried out the CD measurements, analyzed data, and wrote the manuscript. K. F., F. W., C. H. –L., S. L., and M. R. carried out the CD measurements and wrote the manuscript. D. S. –L., E. P., and R. M. carried out the CD measurements. S. Y. supported to prepare the samples and carried out the SDS-PAGE and western blot analyses. M. –A. H. P. designed this research and wrote the manuscript. A. Y. designed this research, carried out the CD measurements, and wrote the manuscript.

Acknowledgments

We thank the anonymous reviewers for their careful reading of the manuscript and valuable comments.

This work was supported in part by the Reimei Research Program of the Japan Atomic Energy Agency and by Grants-in-Aid for Scientific Research, Japan Society for the Promotion of Science (grant number 15K16130). The CD spectroscopy was carried out with the approval of Synchrotron SOLEIL (proposal numbers 20130831 and 20140518).

References

1. De Bont, R., and N. van Larebeke. 2004. Endogenous DNA damage in humans: a review of quantitative data. Mutagenesis 19:169-185.
2. Cadet, J., E. Sage, and T. Douki. 2005. Ultraviolet radiation-mediated damage to cellular DNA. Mutat. Res. 571:3-17.
3. von Sontag, C. 2006. Free-Radical-Induced DNA Damage and Its Repair, Springer, Berlin, pp. 360.
4. Price, B. D. and A. D. D'Andrea. 2013. Chromatin remodeling at DNA double-strand breaks. Cell 152:1344-1354.
5. van Attikum, H., and S. M. Gasser. 2009. Crosstalk between histone modifications during the DNA damage response. Trends Cell Biol. 19: 207-217.
6. Pandita, T. K., and C. Richardson. 2009. Chromatin remodeling finds its place in the DNA double-strand break response. Nucl. Acids Res. 37: 1363-1377.
7. Hunt, C. R., D. Ramnarain, N. Horikoshi, P. Iyengar, R. J. Pandita, J. W. Shay, and T. K. Pandita. 2013. Histone modifications and DNA double-strand break repair after exposure to ionizing radiations. Radiat. Res. 179: 383-392.
8. Gong, F. and K. M. Miller. 2013. Mammalian DNA repair: HATs and HDACs make their mark through histone acetylation. Mutat. Res. Fund. Mol. M. 750: 23-30.
9. Kanaar, R., J. H. J. Hoeijmakers, D. C. van Gent. 1998. Molecular mechanisms of DNA double-strand break repair. Trends Cell Biol. 8:483-489.
10. Lieber, M. R. 2010. The mechanism of double-strand DNA break repair by the nonhomologous DNA end-joining pathway. Annu. Rev. Biochem. 79:181-211.
11. Symington, L. S. and J. Gautier. 2011. Double-strand break end resection and repair pathway choice. Annu. Rev. Genet. 45:247-271.
12. Uziel, T., Y. Lerenthal, L. Moyal, Y. Andegeko, L. Mittelman, and Y. Shiloh. 2003. Requirement of the MRN complex for ATM activation by DNA damage. EMBO J. 22:5612-5621.
13. Burma, S., B. P. Chen, M. Murphy, A. Kurimasa, and D. J. Chen. 2001. ATM phosphorylates histone H2AX in response to DNA double-strand breaks. J. Biol. Chem. 276: 42462-42467.
14. Stewart, G. S., B. Wang, C. R. Bignell, A. M. R. Taylor, and S. J. Elledge. 2003. MDC1 is a mediator of the mammalian DNA damage checkpoint. Nature 421: 961-966.

15. Lou, Z., K. Minter-Dykhouse, S. Franco, M. Gostissa, M. A. Rivera, A. Celeste, J. P. Manis, J. van Deursen, A. Nussenzweig, T. T. Paull, F. W. Alt, and J. Chen. Mol. Cell 21:187-200.
16. Rogakou, E. P., C. Boon, C. Redon, and W. M. Bonner. 1999. Megabase chromatin domains involved in DNA double-strand breaks in vivo. J. Cell Biol. 146:905-915.
17. Ikura, T., S. Tashiro, A. Kakino, H. Shima, N. Jacob, R. Amunugama, K. Yoder, S. Izumi, I. Kuraoka, K. Tanaka, H. Kimura, M. Ikura, S. Nishikubo, T. Ito, A. Muto, K. Miyagawa, S. Takeda, R. Fishel, K. Igarashi, and K. Kamiya. 2007. DNA damage-dependent acetylation and ubiquitination of H2AX enhances chromatin dynamics. Mol. Cell. Biol. 27:7028-7040.
18. Huen, M. S. Y., R. Grant, I. Manke, K. Minn, X. Yu, M. B. Yaffe, and J. Chen. 2007. RNF8 transduces the DNA-damage signal via histone ubiquitylation and checkpoint protein assembly. Cell 131:901-914.
19. Matsuoka, S., B. A. Ballif, A. Smogorzewska, E. R. McDonald III, K. E. Hurov, J. Luo, C. E. Bakalarski, Z. Zhao, N. Solimini, Y. Lerenthal, Y. Shiloh, S. P. Gygi, and S. J. Elledge. 2007. ATM and ATR substrate analysis reveals extensive protein networks responsive to DNA damage. Science 316: 1160-1166.
20. Kolas, N. K., J. R. Chapman, S. Nakada, J. Ylanko, R. Chahwan, F. D. Sweeney, S. Panier, M. Mendez, J. Wildenhain, T. M. Thomson, L. Pelletier, S. P. Jackson, and D. Durocher. 2007. Orchestration of the DNA-damage response by the RNF8 ubiquitin ligase. Science 318:1637-1640.
21. Plans, V., J. Scheper, M. Soler, N. Loukili, Y. Okano, and T. M. Thomson. 2006. The RING finger protein RNF8 recruits UBC13 for lysine 63-based self polyubiquitylation. J. Cell. Biochem. 97: 572-582.
22. Mailand, N., S. Bekker-Jensen, H. Faustrup, F. Melander, J. Bartek, C. Lukas, and J. Lukas. 2007: RNF8 ubiquitylates histones at DNAdouble-strand breaks and promotes assembly of repair proteins. Cell 131:887-900.
23. Stewart, G. S., S. Panier, K. Townsend, A. K. Al-Hakim, N. K. Kolas, E. S. Miller, S. Nakada, J. Ylanko, S. Olivarius, M. Mendez, C. Oldreive, J. Wildenhain, A. Tagliaferro, L. Pelletier, N. Taubenheim, A. Durandy, P. J. Byrd, T. Stankovic, A. M. R. Taylor, and D. Durocher. 2009. The RIDDLE Syndrome protein mediates a ubiquitin-dependent signaling cascade at sites of DNA damage. Cell 136:420-434.
24. Wang, B., S. Matsuoka, B. A. Ballif, D. Zhang, A. Smogorzewska, S. P. Gygi, S. J. Elledge. 2007. Abraxas and RAP80 form a BRCA1 protein complex required for the DNA damage response. Science 316: 1194-1198.
25. Sobhian, B., G. Shao, D. R. Lilli, A. C. Culhane, L. A. Moreau, B. Xia, D. M. Livingston, and R. A. Greenberg. 2007. RAP80 targets BRCA1 to specific ubiquitin structures at DNAdamage sites. Science 316:1198-1202.

26. Kim, H., J. Chen, and X. Yu. 2007. Ubiquitin-binding protein RAP80 mediates BRCA1-dependent DNA damage response. Science 316:1202-1205.
27. Smerdon, M. J. 1991. DNA repair and the role of chromatin structure. Curr. Opin. Cell Biol. 3: 422-438.
28. Soria, G., S. E. Polo, and G. Almouzni. 2012. Prime, repair, restore: H2AX phosphorylation and kinetics of repair of DNA strand breaks in irradiated cervical cancer cell lines. Cancer Res. 64: 7144-7149.
29. Polo, S. E. 2015. Reshaping chromatin after DNA damage: The choreography of histone proteins. J. Mol. Biol. 427:626-636.
30. Goldstein, M., F. A. Derheimer, J. Tait-Mulder, and M. B. Kastan. 2013. Nucleolin mediates nulceosome disruption critical for DNA double-strand break repair. Proc. Natl. Acad. Sci. USA 110:16874-16879.
31. Izumi, Y., S. Yamamoto, K. Fujii, and A. Yokoya. 2015. Secondary structural alterations of histones H2A and H2B in X-irradiated human cancer cells: Altered histones persist in cells for at least 24 hours. Radiat. Res. 184:554-558.
32. Thompson, A., I. Lindau, D. Attwood, P. Pianetta, E. Gullikson, A. Robinson, M. Howells, J. Scofield, K. –J. Kim, J. Underwood, J. Kirz, D. Vaughan, J. Kortright, G. Williams, and H. Winick. 2001. X-ray data booklet, Lawrence Barkeley National Laboratory, California, pp. 1-12 and 1-26.
33. International Commision on Radiation Units and Measurements. 1970. Radiation dosimetry: X-Rays Generated at Potentials of 5 to 150 kV, ICRU Publications, Washington, D.C.
34. Rogakou, E. P., D. R. Pilch, A. H. Orr, V. S. Ivanova, and W. M. Bonner. 1998. DNA double-strand breaks induce histone H2AX phosphorylation on serine 139. J. Biol. Chem. 273:5858-5868.
35. Réfrégiers, M., F. Wien, H. –P. Ta, L. Premvardhan, S. Bac, F. Jamme, V. Rouam, B. Lagarde, F. Polack, J. –L. Giorgetta, J. –P. Ricaud, M. Bordessoule, and A. Giuliani. 2012. DISCO synchrotron-radiation circular-dichroism endstation at SOLEIL. J. Synchrotron Rad. 19:831-835.
36. Karantza, V., A. D. Baxevanis, E. Freire, and E. N. Moudrianakis. 1995. Thermodynamic studies of the core histones: Ionic strength and pH dependence of H2A-H2B dimer stability. Biochem. 34:5988-5996.
37. Micsonai, A., F. Wien, L. Kernya, Y. –H. Lee, Y. Goto, M. Réfrégiers, and J. Kardos. 2015. Accurate secondary structure prediction and fold recognition for circular dichroism spectroscopy. Proc. Natl. Acad. Sci. USA 112:E3095-E3103.
38. Greenfield, N. J. 2006. Using circular dichroism collected as a function of temperature to determine the thermodynamics of protein unfolding and binding interactions. Nat. Protoc. 1:2527-2535.

39. West, H. P., and W. M. Bonner. 1980. Histone 2A, a heteromorphous family of eight protein species. Biochem. 19:3238-3245.
40. Mattiroli, F., M. Uckelmann, D. D. Sahtoe, W. J. van Dijk, and T. K. Sixma. 2014. The nucleosome acidic patch plays a critical role in RNF168-depnedent ubiquitination of histone H2A. Nature Comm. 5: 3291.
41. Greenfield, N., and G. D. Fasman. 1969. Computed circular dichroism spectra for the evaluation of protein conformation. Biochem. 8:4108-4116.
42. Wien, F., A. J. Miles, J. G. Lees, S. V. Hoffmann, and B. A. Wallace. 2005. VUV irradiation effects on proteins in high-flux synchrotron radiation circular dichroism spectroscopy. J. Synchrotron Rad. 12 : 517-523.
43. Placek, B. J., and L. M. Gloss. 2002. The N-terminal tails of the H2A-H2B histones affect dimer structure and stability. Biochem. 41:14960-14968.
44. Davey, C. A., D. F. Sargent, K. Luger, A. W. Maeder, and T. J. Richmond. 2002. Solvent mediated interactions in the structure of the nucleosome core particle at 1.9 Å resolution. J. Mol. Biol. 319:1097-1113; PDB ID: 1KX5.
45. Suto, R. K., M. J. Clarkson, D. J. Tremethick, and K. Luger. 2000. Crystal structure of a nucleosome core particle containing the variant histone H2A.Z. Nat. Struct. Biol. 7:1121-1124; PDB ID: 1F66.
46. Mariño-Ramírez, L., K. M. Levine, M. Morales, S. Zhang, R. T. Moreland, A. Baxevanis, and D. Landsman. 2011. The histone database: an integrated resource for histones and histone fold-containing proteins. Database 2011, bar048.
47. Bradshaw, R. A., W. W. Brickey, and K. W. Walker. 1998. N-terminal processing: the methionine amino peptidase and N^{α}-acetyl transferase families. Trends Biochem. Sci. 23:263-267.
48. Wu, J. M. S. Y. Huen, L. –Y. Lu, L. Ye, Y. Dou, M. Ljungman, J. Chen, and X. Yu. 2009. Histone ubiquitination associates with BRCA1-dependent DNA damage response. Mol. Cell. Biol. 29:849-860.
49. Vijay-Kumar, S., C. E. Bugg, and W. J. Cook. 1987. Structure of ubiquitin refined at 1.8 Å resolution. J. Mol. Biol. 194:531-544; PDB ID: 1UBQ.
50. Lees, J. G., A. J. Miles, F. Wien, and B. A. Wallace. 2006. A reference database for circular dichroism spectroscopy covering fold and secondary structure space. Bioinfomatics 22:1955-1962; protein circular dichroism data bank ID: CD0000071000.
51. Hermans, Jr., J. 1966. Experimental free energy and enthalpy of formation of the α helix. J. Phys. Chem. 70:510-515.
52. Wang, X., S. C. Moore, M. Laszckzak, and J. Ausió. 2000. Acetylation increases the α-helical content of the histone tails of the nucleosome. J. Biol. Chem.275:35013-35020.
53. Sakaue-Sawano, A., H. Kurokawa, T. Morimura, A. Hanyu, H. Hama, H. Osawa, S. Kashiwagi, K. Fukami, T. Miyata, H. Miyoshi, T. Imamura, M. Ogawa, H. Masai, and A.

Miyawaki. 2008. Visualizing spatiotemporal dynamics of multicellular cell-cycle progression. Cell 132:487-498.

Figure legends

Fig. 1. (a) SDS-PAGE analysis of H2A-H2B extracted from core histones in unirradiated cells and 40 Gy irradiated cells after 30 min incubation. The lane labeled “M” refers to the standard molecular weight marker [XL-Ladder (low range); APRO Life Science Institute Inc., Tokushima, Japan]. The lanes labeled “U” and “I” refer to H2A-H2B extracted from unirradiated and irradiated cells, respectively. uH2A(Z) refers to mono-ubiquitinated H2A(Z). (b) Western blotting analysis obtained by using H2AZ antibody.

Fig. 2. CD spectra of H2A-H2B extracted from core histones in unirradiated (Unirrad.; black) and X-irradiated (Irrad.; red) cells, measured at (a) 294, (b) 310, and (c) 330 K. In Fig. 2(a), a CD spectrum of H2A-H2B irradiated with 40 Gy X-rays after extraction from unirradiated cells (13) is also shown (X-irrad. H2A-H2B; blue).

Fig. 3. Temperature dependence of the contents of (a) α-helix, (b) β-strand, (c) turn, and (d) other structures of H2A-H2B extracted from core histones in unirradiated (Unirrad.; open circle) and X-irradiated (Irrad.; filled circle) cells. The contents of X-irradiated H2A-H2B at 294 K are also shown (X-irrad. H2A-H2B; filled triangle).

Fig. 4. Temperature dependence of (a) the CD intensity at 222 nm of H2A-H2B extracted from core histones in unirradiated (Unirrad.; open circle) and X-irradiated (Irrad.; filled circle) cells. Inset: magnification of the unirradiated sample between 320 and 334 K. (b) Temperature dependence of ΔG of both samples, and the corresponding curves of the best fit obtained by the weighted least squares Fig. 4(b).

Fig. 1

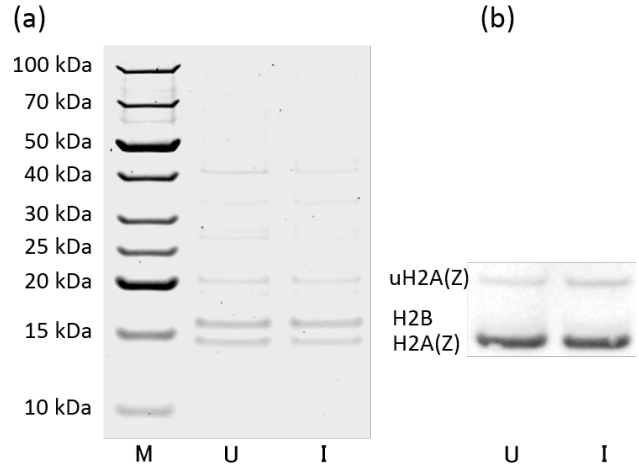
(a)
(b)
100 kDa
70 kDa
50 kDa
40 kDa
30 kDa
25 kDa
20 kDa
15 kDa
10 kDa
M
U
I
uH2A(Z)
H2B
H2A(Z)
U
I

Fig. 2

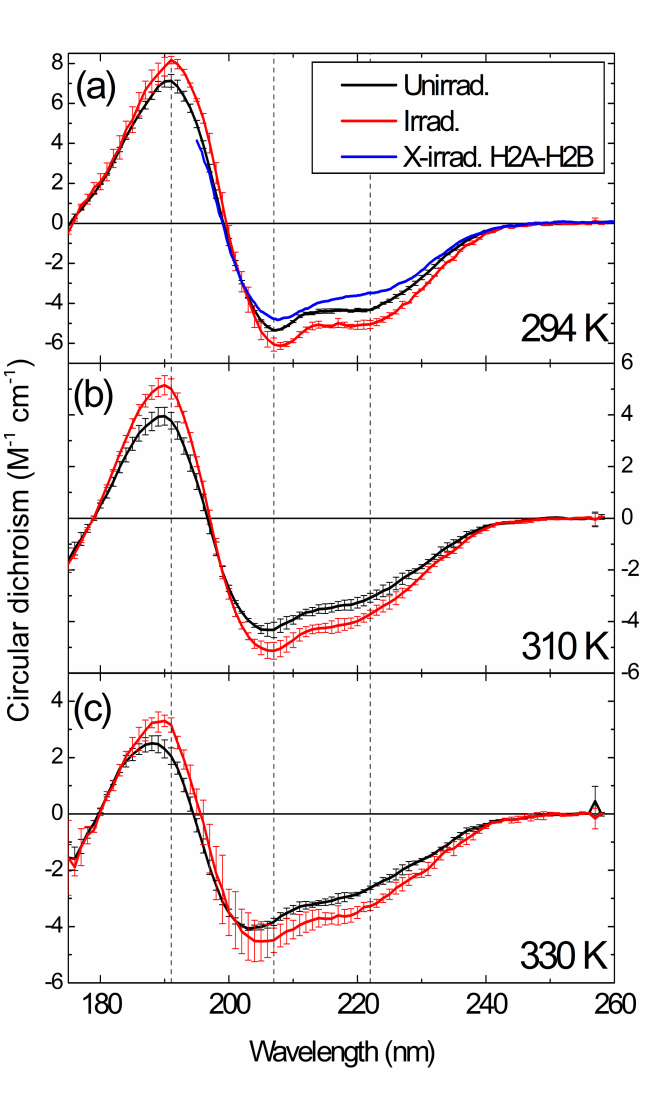
(a)
Unirrad.
Irrad.
X-irrad. H2A-H2B
294 K
(b)
310 K
(c)
330 K
Circular dichroism (M-1 cm-1)
Wavelength (nm)
180
200
220
240
260

Fig. 3

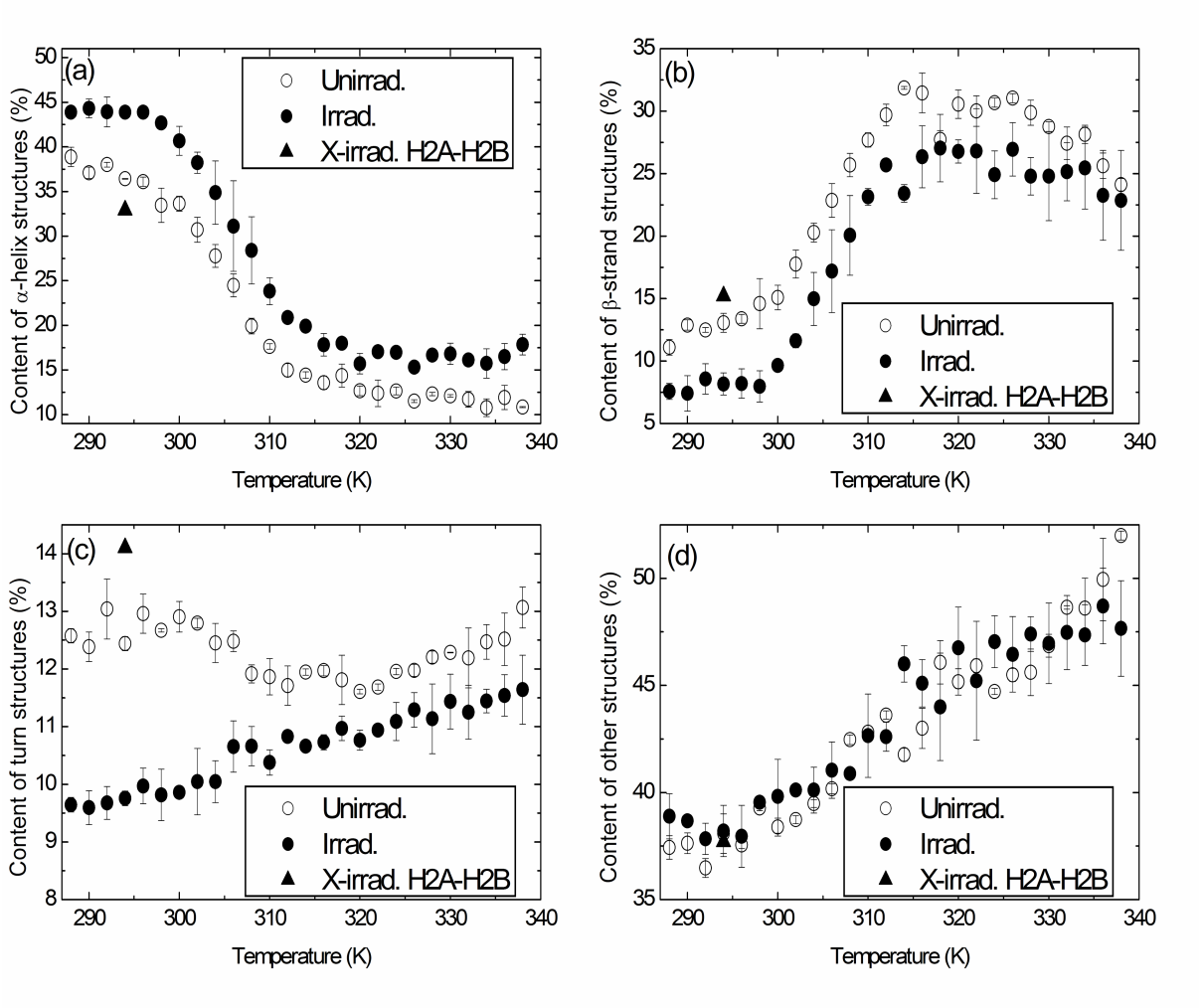
(a)
Unirrad.
Irrad.
X-irrad. H2A-H2B
Content of α-helix structures (%)
Temperature (K)
(b)
Unirrad.
Irrad.
X-irrad. H2A-H2B
Content of β-strand structures (%)
Temperature (K)
(c)
Unirrad.
Irrad.
X-irrad. H2A-H2B
Content of turn structures (%)
Temperature (K)
(d)
Unirrad.
Irrad.
X-irrad. H2A-H2B
Content of other structures (%)
Temperature (K)

Fig. 3

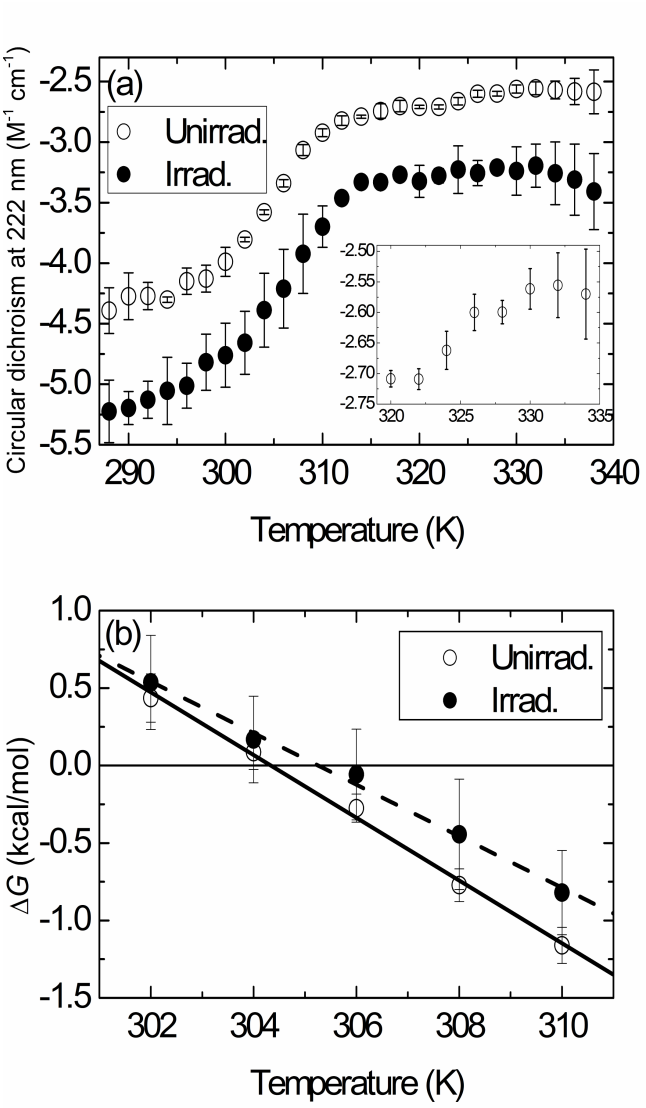
(a)
Unirrad.
Irrad.
Circular dichroism at 222 nm (M^{-1} cm^{-1})
-2.5
-3.0
-3.5
-4.0
-4.5
-5.0
-5.5
290
300
310
320
330
340
Temperature (K)
-2.50
-2.55
-2.60
-2.65
-2.70
-2.75
320
325
330
335
(b)
Unirrad.
Irrad.
ΔG (kcal/mol)
1.0
0.5
0.0
-0.5
-1.0
-1.5
302
304
306
308
310
Temperature (K)

Table 1. Thermodynamic parameters and the midpoint temperature of the lower transition.

	Unirradiated sample	Irradiated sample
Midpoint temperature T_m (K)	304.4±0.3	305.2±0.7
Enthalpy change ΔH (kcal mol^{-1})	66.0±2.4	51.4±2.7
Entropy change ΔS (cal mol^{-1} K^{-1})	217.0±7.8	168.6±8.9

Fig. S1

SDS-PAGE analysis of recombinant H2A and H2B purchased from New England Biolabs, Ltd. The lane labeled “M” refers to standard molecular weight marker [XL-Ladder (low range); APRO Life Science Institute Inc., Tokushima, Japan]. Similar experimental manner described in the manuscript was used.

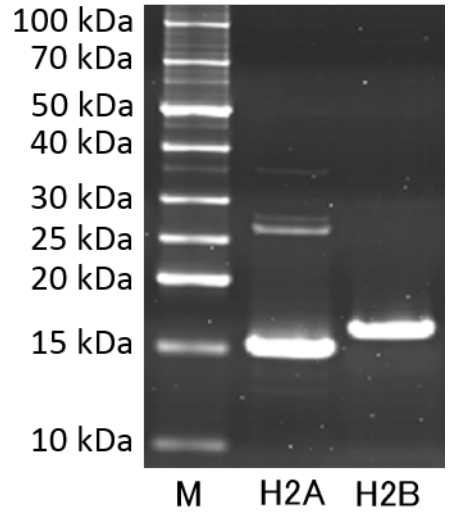

Fig. S2

SDS-PAGE analysis of H2A-H2B extracted from core histones in unirradiated cells (lane "U") and Western blotting analysis obtained by using ubiquitin antibody (lane "W"). The lane labeled "M" refers to standard molecular weight marker [XL-Ladder (low range); APRO Life Science Institute Inc., Tokushima, Japan].

The lane "W" was inserted after adjusting the band positions of the molecular weight markers observed in the SDS-PAGE analysis to those in Western blotting analysis.

For SDS-PAGE analysis, similar experimental manner described in the manuscript was used, but protein bands were stained using SYPRO Ruby Protein Gel Stain (Bio-Rad Laboratories Inc., CA, USA). For Western blotting analysis, a primary antibody, Ubiquitin (P4D1) Mouse mAb (Cell Signaling Technology, Inc., MA, USA), was used at 1:100 dilution. A secondary antibody, ECL Plex goat-α-mouse IgG-Cy5 (GE Healthcare, Buckinghamshire, UK), was used at 1:250 dilution. Images were taken using an Ettan DIGE Imager (GE Healthcare, Buckinghamshire, UK).

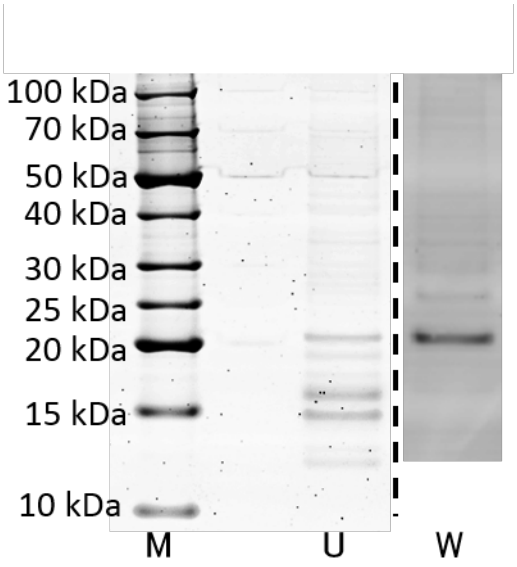

Fig. S3.

SDS-PAGE analysis of H2A-H2B (lane “U”) and that of H3-H4 (lane “H3-H4”) extracted from core histones in unirradiated cells. The lane labeled “M” refers to standard molecular weight marker [XL-Ladder (low range); APRO Life Science Institute Inc., Tokushima, Japan]. Similar experimental manner described in the manuscript was used, but protein bands were stained using SYPRO Ruby Protein Gel Stain (Bio-Rad Laboratories Inc., CA, USA).